Smart Materials and Structures

PAPER

A study of the heat transfer properties of CIP doped magnetorheological elastomers

To cite this article: Hongmei Zhong *et al* 2019 *Smart Mater. Struct.* **28** 025027

View the article online for updates and enhancements.

This content was downloaded from IP address 218.22.21.24 on 15/03/2019 at 01:56

IOP Publishing Smart Materials and Structures
Smart Mater. Struct. **28** (2019) 025027 (8pp) https://doi.org/10.1088/1361-665X/aaf36e

A study of the heat transfer properties of CIP doped magnetorheological elastomers

Hongmei Zhong[1], Yu Pei[1], Zhijiang Hu[1], Peng Zhang[1], Jian Guo[1], Xinglong Gong[2] and Yang Zhao[1]

[1] CAS Key Laboratory of Mechanical Behavior and Design of Materials, Department of Precision Machinery and Precision Instrumentation, University of Science and Technology of China, Hefei, Anhui 230027, People's Republic of China
[2] CAS Key Laboratory of Mechanical Behavior and Design of Materials, Department of Modern Mechanics, University of Science and Technology of China, Hefei, Anhui 230027, People's Republic of China

E-mail: yangz1@ustc.edu.cn

Received 8 September 2018, revised 24 October 2018
Accepted for publication 23 November 2018
Published 21 January 2019

Abstract

This work investigates the enhancement of thermal transport in polydimethylsiloxane (PDMS) thin films with aligned carbonyl iron particles (CIP) embedded, also known as magnetorheological elastomers (MREs). The flash method is used to measure the effective thermal conductivity of PDMS/CIP thin films in the direction parallel to the magnetic field. Under an external magnetic field, the CIPs form chain-like structures, which become effective thermal paths inside the composites. Hence, a significant increase in the thermal conductivity of aligned MREs has been achieved compared with the composites prepared without a magnetic field. The effects of the volume fraction of CIP and pre-structured magnetic flux density have also been studied. The increase in the CIP volume fraction from 5% to 20% brings about a twofold improvement in the thermal conductivity of the aligned MREs. For 2.5 μm CIP doped MREs with a volume fraction of 10%, when the pre-structured magnetic flux density changes from 0 mT to 100 mT, the thermal conductivity k increases by approximately 50%. However, a further increase in the magnetic field intensity only leads to a slight increase in k. Scanning electron microscopy (SEM) inspections demonstrate that the chain length keeps growing with the strength of the pre-structured magnetic field while the structure transition turns into lateral congregation as the strength of the pre-structured magnetic field reaches 100 mT. A finite element method (FEM) model is proposed to investigate in detail the relationship between the MREs' thermal conductivity and inner chains. This work provides an effective way to improve thermal conductivity of MREs used for electromagnetic radio-absorbers and builds a connection between the thermal properties of MREs and their inner microstructures.

Keywords: magnetorheological elastomers, thermal conductivity, finite element

(Some figures may appear in colour only in the online journal)

1. Introduction

Magnetorheological elastomers (MREs), which are prepared by dispersing micron-sized magnetic particles into a polymer matrix, have attracted great interest as a novel smart material in recent years, for their rheological properties can be controlled by an external magnetic field [1–6]. Based on the inner microstructures, MREs are classified into isotropic MREs and anisotropic MREs. In the former, particles are homogeneously dispersed, while in the latter, particles are oriented into chain-like or columnar structures along the magnetic field direction during the curing process [7]. Most of the previous work merely focused on enhancing and manipulating the mechanical properties of MREs so as to meet the requirements in conventional practical application, such as vibration control, the automotive industry, absorbers, etc [8–12].

 © 2019 IOP Publishing Ltd Printed in the UK

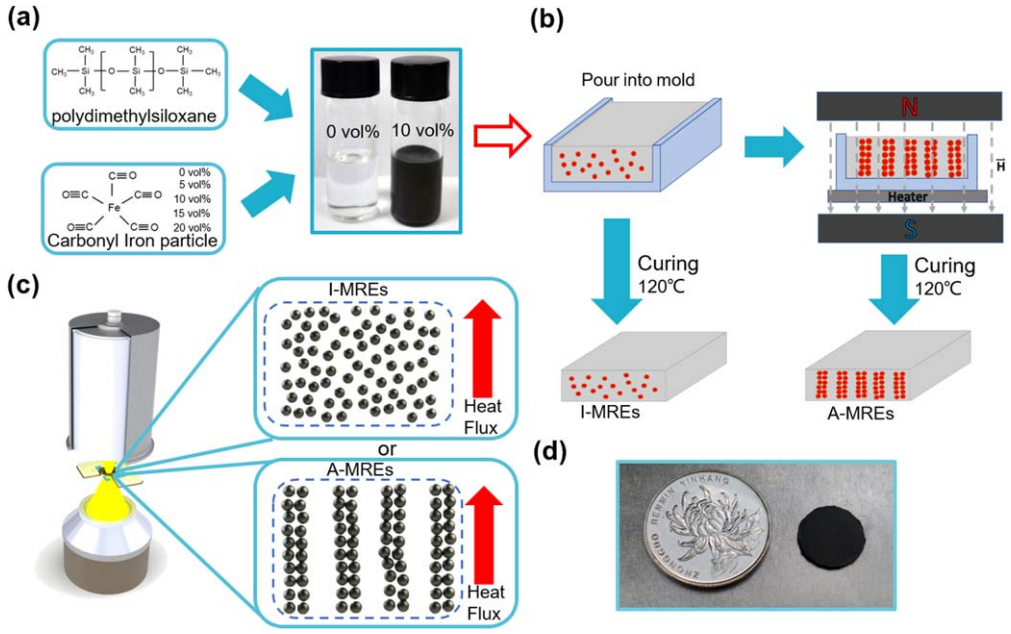

Figure 1. Sample preparation and thermal measurement. (a), (b) the experimental procedure for preparing MREs. (c) The experimental setup of the thermal measurement. (d) An MRE sample for thermal measurement.

More recently, many novel applications have been proposed. An MRE film with tunable wetting and adhesion properties was used as a superhydrophobic surface [13], and a sensitive and reversible MRE strain sensor was proposed by Ge *et al* [14]. Moreover, Sedlacik *et al* [15] have successfully used MREs for absorbing electromagnetic (EM) radiation in the ultra-high frequency band through various loss mechanisms associated with magnetization and electric polarization processes. Martin *et al* [16] further found that anisotropic MRE-based radio-absorbers (RAs) had superior EM shielding capabilities in the microwave frequency range compared to their isotropic analogues. These MRE-RAs are of great importance because, with the development of information technology and microwave communications, a large number of harmful EM signals have radiated into our surroundings. MRE-RAs convert EM energy into Joule heat. Therefore, the thermal conductivity k of the MRE materials is considered as an important factor. Low-k materials fail to effectively dissipate the generated heat, thus causing local overheating, which may shorten the service life of these devices.

Although enhancing the thermal conductivity of materials through the embedding of randomly dispersed highly conductive fillers has been extensively studied in in recent years [17–19], research related to the thermal properties of MREs is very limited. Boudenne *et al* [20] noticed that the thermal behavior of silicone-nickel composite had been greatly improved by using magnetic fields during preparation. Su *et al* [21] showed a thermal conductivity increase of polydimethylsiloxane (PDMS)/Ni composites with increasing filler volume fraction. Chung *et al* [22] concluded that the linear alignment of thermally conductive fillers contributed to thermal conductivity enhancement of the Al_2O_3-containing composites. It is found that the microstructures of MREs have a strong influence on their macroscopic mechanical response [23, 24]. However, few works have been conducted to build a relationship between the MRE microstructure and its thermal properties. To this end, the thermal properties of MREs and their connections with inner microstructures become the central focus of this research.

In this work, the thermal transport performances of isotropic and anisotropic PDMS/CIP MREs were both studied. The influence of filler volume fraction, pre-structured magnetic field intensity on the inner microstructure and thermal properties of the PDMS/CIP MREs were also investigated, and the results were compared with theoretical predictions. Furthermore, an finite element method (FEM) model was proposed to explain the thermal behavior of the MREs under different pre-structured magnetic fields.

2. Experimental section

2.1. Sample preparation

PDMS (Sylgard 184, Dow Corning GmbH, USA) precursor and curing agent were selected as a matrix. Carbonyl iron particles (CIP) were used as received as magnetic fillers, which were spherical shaped with a density of 7.649 g cm^{-3} (BASF GERMANY). CIPs with an average diameter of 2.5 μm and 6 μm were both studied. The MRE preparation procedure is shown in figures 1(a) and (b): first, PDMS precursor and curing agent were mixed in the proportion of 10:1 in weight at room temperature and then loaded with the CIPs. After adding CIPs, the mixture was sonicated for 10 min to disperse the particles homogeneously avoiding sedimentation. Then, the mixture was put into a vacuum chamber for 30 min to reduce air bubbles. Second, the mixture was transferred into an aluminum mold to define the sample size as 5 cm × 5 cm × 1 mm. For isotropic MREs (I-MREs), the

molded samples were directly cured for 25 min at 120 °C. For anisotropic MREs (A-MREs), samples were moderately cured in a homemade magneto-heat-coupled device with a preset magnetic field in the cross plane direction at 80 °C for 10 min to respond to the external magnetic field; then the curing continued at 120 °C for 20 min without the presence of the magnetic field for quick curing. The intensity of the magnetic field varied from 0 mT to 800 mT, and MRE samples with CIP volume fractions ranging from 5%, 10%, 15%, and 20% were fabricated.

2.2. Characterization

The morphology of the MRE samples was inspected under an environment scanning electron microscope (SEM). The thermal conductivity was tested using the flash method (NETZSCH LFA 467 hyperflash). Figures 1(c) and (d) illustrate the measurement setup and the sample configurations. The xenon source emits a pulse of light at an instant, and evenly irradiates the lower surface of the disk-shape sample, so that the surface layer absorbs light energy and the temperature rises instantaneously. This surface acts as a hot end to conduct energy in a one-dimensional heat conduction manner to the cold end (upper surface). Thermal diffusivity D and specific heat C were determined based on the temperature response at the upper surface measured by an infrared (IR) detector. The density of the sample ρ can be calculated based on the Archimedes principle. Combining D, C and ρ, the thermal conductivity k of the sample can be determined as:

$$k = D \times C \times \rho \tag{1}$$

3. Results and discussion

3.1. Effect of CIP volume fraction

To study the effect of CIP volume fraction on MRE thermal conductivity, 2.5 μm CIP was chosen, and the pre-structured magnetic field was set to be 300 mT. MRE samples with CIP volume fractions ranging from 5%, 10%, 15%, and 20% were both studied. The preparation details are illustrated in section 2.1. With the given measurement setup, the measured thermal conductivity k is in the cross plane direction, which is aligned with the pre-structured magnetic field direction for A-MREs. The error of k measured by NETZSCH LFA 467 is generally defined as ±5% according to LFA specification. The results for A-MREs and I-MREs with various CIP volume fractions are shown in figure 2. The thermal conductivity for pure PDMS is measured to be 0.15 W mK^{-1}, similar to previous reports [21, 25]. As can be seen in figure 2(a), for both A-MREs and I-MREs, the higher the CIP volume fraction, the larger k is. In addition, for samples with the same CIP volume fraction, A-MREs pre-structured under an external magnetic field achieve a considerably higher conductivity compared with I-MREs. This is because when the dipolar interaction energy becomes sufficiently strong under magnetic field, the magnetic particles assemble chain-like structures, which form thermal transport paths in the composites [26]. With the number of particles per unit volume increasing, the chance of the particles forming a chain in the presence of an external magnetic field grows. Therefore, the relative enhancement, namely the ratio of k of A-MREs to that of I-MREs with the same CIP volume fraction, becomes larger with increasing CIP volume fraction, which has been demonstrated previously [20].

A Maxwell model and an FEM numerical model are presented to compare with the experimental results. The Maxwell model considers a dilute distribution of spherical particles embedded in a continuous matrix. The effective electrical conductivity of the composite can be derived based on the theory of electric potential that satisfies the Laplace equation [27–29]. Due to the analogy between the electric potential and the temperature of steady heat conduction, it applies equally well to the thermal conductivity. The effective thermal conductivity can then be described as [29]:

$$k_{\text{eff}} = k_{\text{m}} \frac{2k_{\text{m}} + k_{\text{f}} - 2\phi(k_{\text{m}} - k_{\text{f}})}{2k_{\text{m}} + k_{\text{f}} + \phi(k_{\text{m}} - k_{\text{f}})} \tag{2}$$

where k_{m} and k_{f} denote the thermal conductivity of polymer matrix and fillers, respectively, and ϕ denotes the filler volume fraction. The filler (CIP) conductivity, $k_{\text{f}} = 78.4$ W mK^{-1}, and matrix (PDMS) conductivity, $k_{\text{m}} = 0.15$ W mK^{-1}. The conductivities of the composites with various filler volume fractions are calculated using the Maxwell model and plotted in figure 2(a) (red solid line). As shown, the Maxwell model provides a fairly good prediction for randomly dispersed MREs (I-MREs). It should be noted that a previous study has shown an underestimation of the model [21]. The possible reason is that the samples studied in this work are lower filler volume fraction composites (<20%). The fillers are more easily dispersed to avoid interactions with each other, which agrees with the hypothesis of the Maxwell model that thermal interactions among particles can be ignored [27]. As the CIP volume fraction becomes higher, the chances of particles in contact with each other gets larger and the direct thermal transport from particle-to particle cannot be ignored [30].

For A-MREs, a numerical model implemented on a COMSOL platform Version 5.0 was developed to carry out thermal analysis within a representative cuboid of the composite. Three-dimensional models have been used to simulate the microstructure of composite materials for various filler volume fractions. They consist of spheres with a diameter of 2.5 μm along the magnetic field direction in a cuboid. The PDMS interfacial layer between two particles was assumed to be 0.002 μm [21]. The interfacial layer also exists between the cuboid top/bottom surfaces and particles. Since continuous chains were formed along the sample thickness direction without breaking points, every part in the chain was the same. Therefore, we chose four particles to conduct heat transfer numerical analysis. The temperatures at the top and bottom surface of the cuboid were prescribed as T_1 and T_2. The other surfaces parallel to the direction of the heat flow were all assumed adiabatic, as depicted in figure 2(c). By varying the cross-sectional area, denoted as A, of the cuboid, different volume fractions could be achieved. The effective thermal

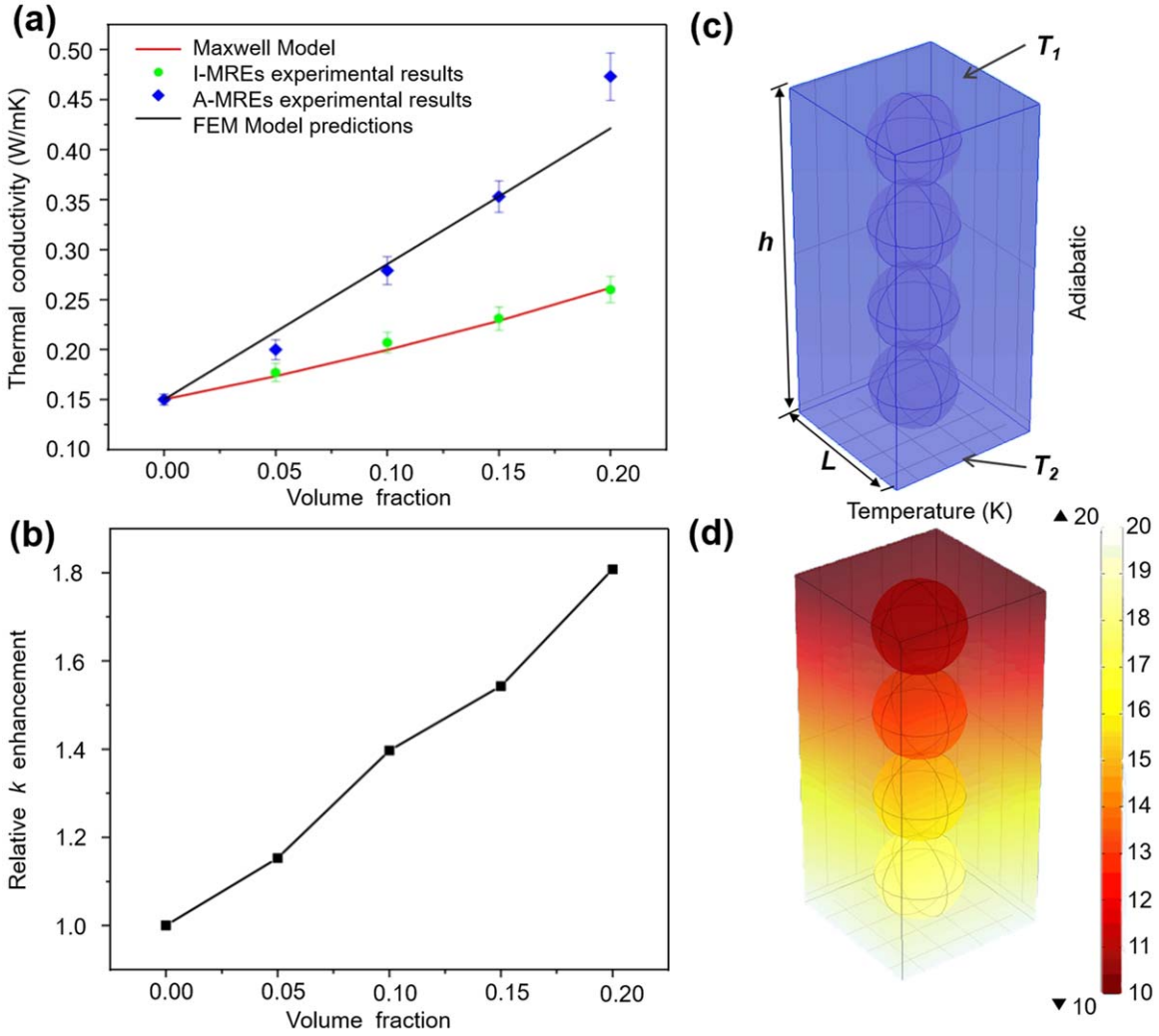

Figure 2. (a) The measured thermal conductivity for A-MREs and I-MREs; the Maxwell and FEM models are shown for comparison. (b) The relative enhancement with respect to CIP loading. (c) Boundary conditions of the finite-element model. (d) The temperature distribution when $\phi = 0.15$.

conductivity is then determined by:

$$k_{\text{eff}} = \frac{Q/A}{(T_2 - T_1)/h} \tag{3}$$

where Q is the total heat flow across the bottom surface of a cuboid and h is the height of the unit cell. The total heat flowing into the cuboid can be obtained by integrating the local heat flux over the cross-sectional area:

$$Q = \int_0^L \int_0^L -k_{\text{m}} \left(\frac{\partial T_{\text{m}}}{\partial z} \right) |_{z=0} \text{d}x\text{d}y \tag{4}$$

where k_{m} and T_{m} denote the thermal conductivity and temperature of the matrix.

As illustrated in figure 2(a), the experimental results do not exactly fall into the predictions (black solid line). This is because the numerical model assumes that the number of thermal paths increase linearly with the increasing volume fraction, leading to the linear increase in the thermal conductivity. However, when in actual preparation, particles in lower volume fraction composites find it more difficult to form chains than in higher ones under same preparation conditions, since the distance between the particles is much larger for lower volume fraction samples, which means particles need to travel longer paths to join together and form chains. Therefore, the experimental data indicates an increasing enhancement trend as the CIP volume fraction increases, as shown in figure 2(b).

SEM images of chain-like aggregates were demonstrated in the microstructures of the PDMS/CIP composites, as depicted in figure 3. Samples were cut into two halves along the alignment direction, as shown in figure 3(a), so the cross plane morphology could be observed. Figures 3(b)–(d) show the images of the isotropic samples, and figures 3(e)–(g) indicate the anisotropic samples. It should be noted that some malposition of the particles may have been caused during the cutting process. Nevertheless, the presented images indicate particle-to-particle proximities to some extent. The comparison of figures 3(b)–(d) and (e)–(g) confirms the formation of chain-like structures under a magnetic field, and with the filler concentration getting higher, the chain structure tends to be more dense and obvious.

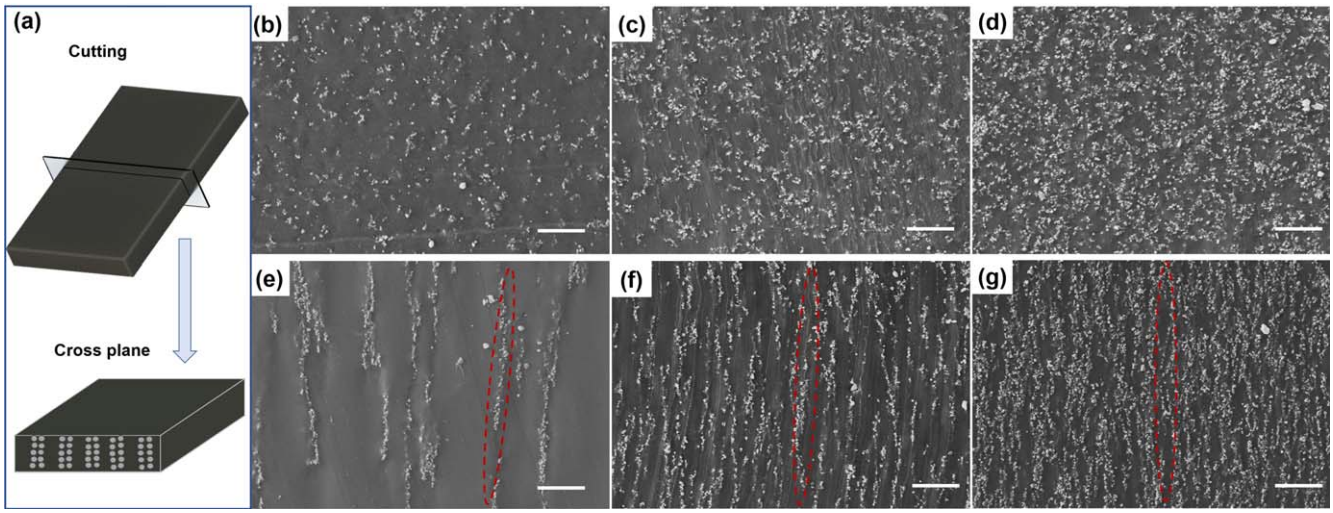

Figure 3. SEM images of the internal microstructure of the composites prepared under 300 mT with different particle volume fractions: (a) cutting for cross plane structures; (b) $\phi = 0.05$ isotropic MRE; (c) $\phi = 0.10$ isotropic MRE; (d) $\phi = 0.20$ isotropic MRE; (e) $\phi = 0.05$ anisotropic MRE; (f) $\phi = 0.10$ anisotropic MRE; and (g) $\phi = 0.20$ anisotropic MRE. The scale bar is 50 μm.

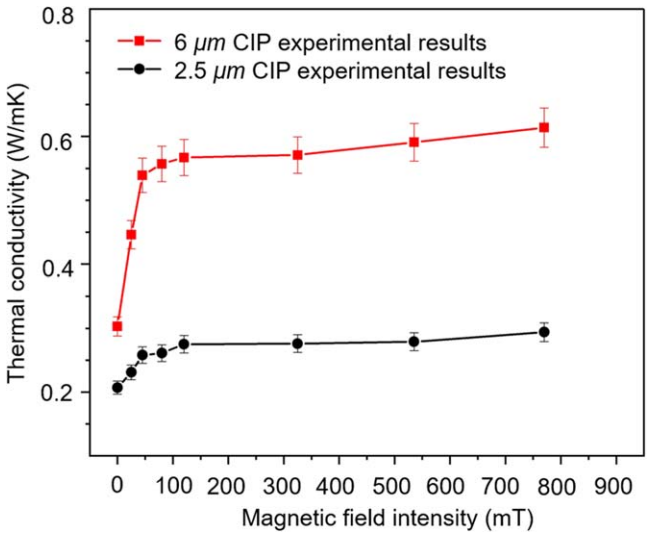

Figure 4. The k of A-MREs with a CIP volume fraction of 10% as a function of increasing pre-structured magnetic fields.

3.2. Effects of pre-structured magnetic field intensity

To obtain a better understanding of the effect of field-induced chain structures on k enhancement, we also measured the thermal conductivity of MREs prepared under different magnetic field H with different filler sizes: 2.5 μm CIP and 6 μm CIP were both studied. CIP volume fraction was maintained at 10% and the pre-structured magnetic field intensity varied from 0 to 800 mT. Figure 4 shows the variation in k to H for both particles. MREs with large sized particles (6 μm) embedded possess better thermal transfer ability compared with small sized particles (2.5 μm), which is similar to the reports that show a decrease in k with the decrease in particle size in nanofluids [31, 32]. The increase in k with particle size may originate from the kinetic growth of small particles into fractal-like aggregates in the suspensions, where the process can be diffusion or reaction limited [33]. Moreover, as H increases from zero to 100 mT, k enhances sharply. But k experiences a slight increase after 100 mT.

Cross sections of samples were also examined under SEM to further illustrate morphology differences behind the k enhancement phenomenon, as shown in figure 5. As the external magnetic field is slowly increased from zero to 800 mT, the MRE inner structures go through different transitions. First, under low H (<100 mT), all the random particles start to form short tip-to-tip structures along the field direction. By increasing H, short chains tend to grow longer (figure 5(c)). Then, when H reaches 100 mT, long through chains will be formed that have equal length to sample thickness and are parallel to the magnetic direction (figure 5(d)). If H keeps increasing, as the chain length cannot be increased further due to the limitation of the sample thickness, chains begin to aggregate laterally then form clusters. Thus the enhancement of k under low H could be seen as the results of the growing length of the heat transfer paths, while the small increase in k under high H indicates that the lateral aggregation enables cross talk between the chains and contributes mildly to thermal transport.

A kinetic model was developed to predict the chain length for A-MREs prepared under various low H. Magnet particle transport in the incompletely cured PDMS is governed by (a) magnetic force, (b) viscous drag, (d) gravity and (e) thermal kinetics (Brownian motion). For 2.5 μm particles, the Brownian motion can be ignored [34]. The gravitational force on the iron particle is about 6.3×10^{-14} N, while the viscous drag force is over 10^{-10} N. Therefore, it can also be neglected [35]. The interaction between two particles leads to the formation of pair aggregates in very short timescales after the application of the magnetic field (less than 1 s). Then, the aggregates follow a deterministic drift in the direction of the magnetic field. As time goes on, we assume a tip-to-tip and pair-to-pair collision, making longer aggregates along the field direction until the viscosity of the PDMS limits the particle movement. The process is shown in figure 6.

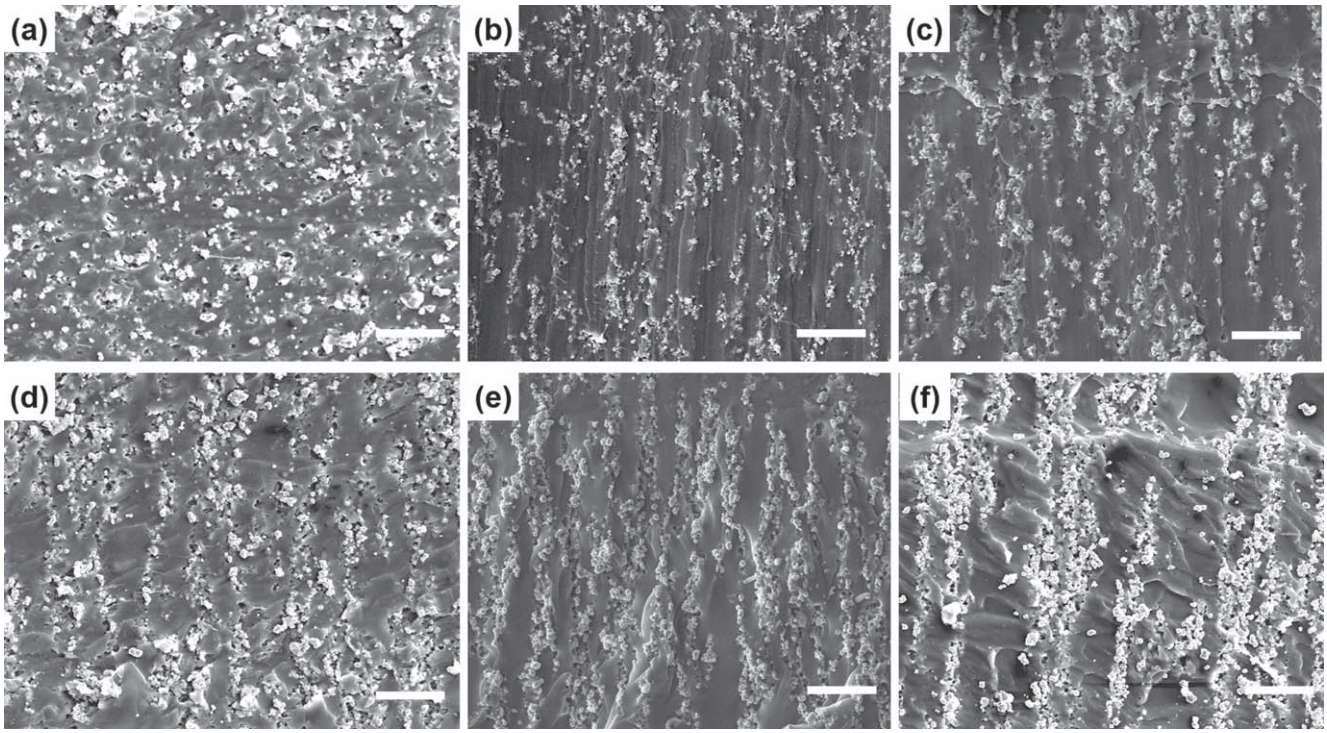

Figure 5. SEM images of the internal microstructure of MRE samples with a CIP volume fraction of 10% prepared under different magnetic fields: (a) 0 mT, (b) 20 mT, (c) 40 mT, (d) 100 mT, (e) 300 mT and (f) 800 mT. The scale bar is 50 μm.

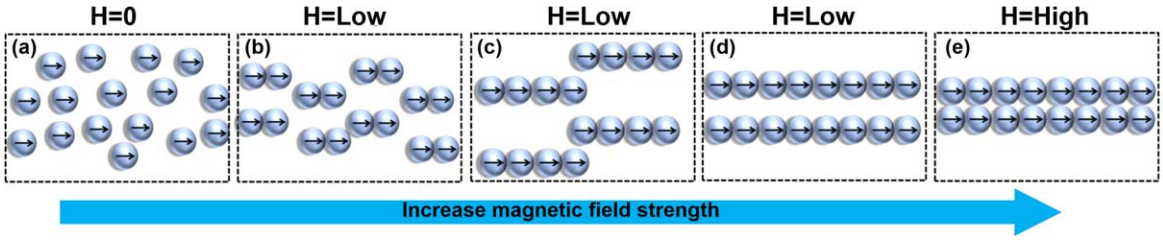

Figure 6. The illustration of tip-to-tip and pair-to-pair chain formation with the increase in the pre-structured magnetic field intensity.

The drag force is taken as Stokes drag on an elongated aggregate made of sphere particles [35, 36].

$$F = \frac{3\pi\eta a v}{\frac{3}{(2s)}\left[\ln\left(2s - \frac{1}{2}\right)\right]} \tag{5}$$

where s is the number of particles in an individual aggregate, η is the viscosity of the matrix material and a (=2.5 μm) and v are the diameter and velocity of the filler particles, respectively. The aggregate of s particles can be considered as an effective sphere with diameter $a_{\text{eff}} = s^{1/3}a$ [37]. Therefore, the magnitude of the induced dipole moment of the aggregate can be obtained as:

$$m = \frac{\pi}{6}(s^{1/3}a)^3\chi H_0 \tag{6}$$

where χ (10^{-4}) [38] is the effective magnetic susceptibility of an individual particle, and H_0 is the magnitude of the external magnetic field. The interaction energy between two dipoles with magnitude m and distance r is given by

$$U_{\text{mag}} = -\frac{m^2\mu_0}{4\pi r^3} \tag{7}$$

where μ_0 (=$4\pi \times 10^{-7}$) is the magnetic permeability in free space. To simplify the calculation, only the case of maximum attraction between the particles, that is when vector r is parallel to the magnetic field direction, is taken into account. The balance between magnetic force and viscous drag sets the timescale for aggregation [39]:

$$\frac{3\pi\eta a}{\frac{3}{(2s)}\left[\ln\left(2s - \frac{1}{2}\right)\right]}\frac{\mathrm{d}r}{\mathrm{d}t} = -\frac{\mathrm{d}U_{\text{mag}}}{\mathrm{d}r} \tag{8}$$

Initially (before applying the magnetic field), particles in a random distribution are separated at a typical distance $n^{-1/3}$, where n is the number of particles per unit volume (10^{16} for 10 vol% CIP with a diameter of 2.5 μm). For aggregates with s particles, the distance is increased to $d \approx \left(\frac{n}{s}\right)^{-1/3}$. The time for two aggregates to form a longer one can then be obtained

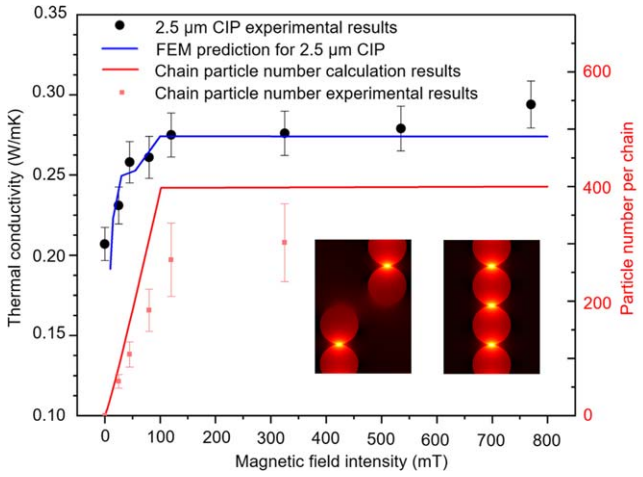

Figure 7. A comparison of the experimental results and the FEM prediction for 2.5 μm CIP. The inserts are heat flux distributions.

by integrating equation (8) for the motion of the particles from an initial distance $r = d$ to a final distance $r = a_{\text{eff}}$ [39]. We obtain:

$$t = \frac{36\eta \Big/ \frac{3}{2s}\left[\ln(2s - \frac{1}{2})\right]}{5\mu_0 \chi^2 n^{5/3}\left(\frac{1}{s}\right)^2 a^5 H^2} \tag{9}$$

The maximum s is 400 because the thickness of the composites is 1000 μm. t is taken as the total curing time under magnetic field 600 s. The viscosity η of the PDMS changes from 3.5 Pa·s to infinity during the curing process (80 °C, 600 s) [40]. Assuming the correlation between PDMS viscosity and curing time is $\eta(t) = 3.5 \times e^{t/\tau}$. A previous research showed that τ was 65 s when the curing temperature was 60 °C [41], it took 3 h for PDMS to be completely cured at 60 °C [42]. And when the curing temperature is increased to 80 °C, the time for PDMS to be completely cured is then reduced to 2.5 h [43]. Thus, it is reasonable to assume τ to be 55 s at 80 °C. To simplify the calculation, viscosity is taken as the average results over a 600 s time period, which is about 3000 Pa·s . According to equation (9), the particle number s within a chain under various intensity H of pre-structured magnetic field can be obtained; the results are shown in figure 7 (red solid line). At the beginning, the chain length growth corresponds to the transmission from figure 6(a) to figure 6(d), which then causes the thermal conductivity to soar. When the intensity of the magnetic field is around 100 mT, chains that link the bottom and the top of the sample are formed, as depicted in figure 6(d). The chain length can no longer increase and thus k is saturated.

A statistical method was also used to obtain the average lengths of the particle chains of MREs prepared under different magnetic fields for comparison. The composites were cut into pieces along the direction of the CIP chains. Dozens of SEM images were obtained at the magnification of 100. Then, image processing was used to separate CIP chains from the PDMS matrix. The real lengths of the CIP chains could be simply calculated according to the scale bar. Lengths of 130 chains were counted for each sample. To minimize statistical error, the chosen chain should be continuous and parallel. An aberrancy of less than 5° was acceptable [44]. The results are shown in figure 7 (red squares). The counted chain lengths are smaller than the theoretical ones and slightly over half of the predicted lengths. This is because malposition of the particles has been caused during the cutting process. Some continuous and straight chains could inevitably be broken due to particle malposition, especially for long chains. So, statistically, the average length for some chain pieces and some unbroken chains would be slightly over half the predicted chain length. Although there is underestimation, the presented results indicate particle length growth until its saturation with the magnetic field intensity to some extent.

With the chain particle number obtained under a certain intensity of magnetic field, the previous numerical method implemented on the COMSOL platform has been further developed to predict and understand the cross plane thermal conductivity of the A-MREs prepared under various magnetic fields, of which the thickness is 1 mm (400 particles along the thickness direction). After 100 mT, the chain length would be maintained, and the chains form columns that run through the composites. The diameter of the particles is 2.5 μm and the volume fraction is maintained at 10%. The thermal conductivities of the controlled cells from the simulation results are plotted in figure 7 (blue solid line), which reveals that for the magnetically aligned particles, there is a good agreement between the numerical prediction and experimental measurements during the chain length increasing period. The underestimate for high H is because, in the simulation, the particle chains and polymer channels are assumed to be well separated from each other even when columns are formed, therefore, the thermal conductivity reaches its saturation when the chain length reaches its sample thickness limits. In real situations, more complicated heat transfer paths may be formed between chains that bundle together. The inserts are the detailed heat flux distribution around the particle contacting and gap area. Compared with continuous chains, the gap between two short chains will interfere with the heat transfer path and lower the thermal conduction efficiency.

4. Conclusion

Both isotropic and anisotropic PDMS/CIP MREs were prepared. Thermal conductivity measured by LFA showed a clear enhancement with increasing CIP volume fraction. Moreover, A-MREs had a much higher thermal conductivity than I-MREs. The morphology indicated that chain structures formed under a magnetic field contributed to the relative high k of A-MREs, and higher volume fractions resulted in longer and denser chains, thus more efficient heat transfer paths. The relationship between thermal conductivity and pre-structured magnetic field intensity was also studied. Thermal conductivity increased sharply under low H, and very slightly when H was high. The SEM analysis of the composites revealed that a higher magnetic field led to a longer chain structure until it crossed through the whole thickness of the sample. Then, the chains would gather together and form a thicker one. A numerical model based on column structure

was built to predict the thermal conductivity enhancement with respect to field intensity increase, and a good agreement with the experimental results was achieved for aligned PDMS/CIP MREs. In conclusion, these results confirmed that the chain structure formation is essential in the thermal conductivity enhancement of MREs. On the other hand, the lateral congregation of aligned particle chains only slightly enhances thermal transport in the composites.

Acknowledgments

This work was supported by the National Natural Science Foundation of China (No.51732006, No.15572311 and No.11772321), the National Science Foundation for Young Scientists of China (No.51707001) and the Chinese 1000 Young Talented Program. The authors wish to thank the Experimental Center of Engineering and Material Science of USTC. The authors also wish to thank the USTC Center for Micro- and Nanoscale Research and Fabrication.

ORCID iDs

Xinglong Gong https://orcid.org/0000-0001-6997-9526
Yang Zhao https://orcid.org/0000-0002-3962-2793

References

[1] Ginder J M, Nichols M E, Elie L D and Tardiff J L 1999 *Proc. SPIE* **3675** 131–9
[2] Bellan C and Bossis G 2002 *Electrorheological Fluids And Magnetorheological Suspensions* (Singapore: World Scientific) pp 507–13
[3] Zhou G 2003 *Smart Mater. Struct.* **12** 139
[4] Rigbi Z and Jilken L 1983 *J. Magn. Magn. Mater.* **37** 267–76
[5] Gong X, Zhang X and Zhang P 2005 *Polym. Test.* **24** 669–76
[6] Yu M, Qi S, Fu J, Yang P and Zhu M 2015 *Smart Mater. Struct.* **24** 045009
[7] Wu J, Gong X, Fan Y and Xia H 2012 *J. Appl. Polym. Sci.* **123** 2476–84
[8] Li W and Du H 2003 *Int. J. Adv. Manuf. Technol.* **21** 508–15
[9] Carlson J D and Jolly M R 2000 *Mechatronics* **10** 555–69
[10] Lerner A A and Cunefare K 2008 *J. Intell. Mater. Syst. Struct.* **19** 551–63
[11] Li Y, Li J, Li W and Samali B 2013 *Smart Mater. Struct.* **22** 035005
[12] Li W, Yao G, Chen G, Yeo S and Yap F 2000 *Smart Mater. Struct.* **9** 95
[13] Lee S, Yim C, Kim W and Jeon S 2015 *ACS Appl. Mater. Interfaces* **7** 19853–6
[14] Ge L, Gong X, Wang Y and Xuan S 2016 *Compos. Sci. Technol.* **135** 92–9
[15] Sedlacik M, Mrlík M, Babayan V and Pavlínek V 2016 *Compos. Struct.* **135** 199–204
[16] Cvek M, Moucka R, Sedlacik M, Babayan V and Pavlínek V 2017 *Smart Mater. Struct.* **26** 095005
[17] Fang H, Zhang X, Zhao Y and Bai S L 2017 *Compos. Sci. Technol.* **152** 243–53
[18] Lee G W, Park M, Kim J, Lee J I and Yoon H G 2006 *Composites A* **37** 727–34
[19] Zhou Y, Bai Y, Yu K, Kang Y and Wang H 2013 *Appl. Phys. Lett.* **102** 252903
[20] Boudenne A, Mamunya Y, Levchenko V, Garnier B and Lebedev E 2015 *Eur. Polym. J.* **63** 11–9
[21] Su J, Liu X, Charmchi M and Sun H 2016 *Int. J. Heat Mass Transfer* **97** 645–52
[22] Chung J Y, Lee J G, Baek Y K, Shin P W and Kim Y K 2018 *Composites B* **136** 215–21
[23] Chen L, Gong X and Li W 2007 *Smart Mater. Struct.* **16** 2645
[24] Farshad M and Benine A 2004 *Polym. Test.* **23** 347–53
[25] Li B, Dong S, Wu X, Wang C, Wang X and Fang J 2017 *Compos. Sci. Technol.* **147** 52–61
[26] Philip J, Shima P and Raj B 2008 *Appl. Phys. Lett.* **92** 043108
[27] Maxwell J C 1881 *A Treatise on Electricity and Magnetism* vol 1 (Oxford: Clarendon)
[28] Turian R M, Sung D J and Hsu F L 1991 *Fuel* **70** 1157–72
[29] Zhou H, Zhang S and Yang M 2007 *Compos. Sci. Technol.* **67** 1035–40
[30] Kumlutas D and Tavman I H 2006 *J. Thermoplastic Compos. Mater.* **19** 441–55
[31] Shalkevich N, Escher W, Burgi T, Michel B, Si-Ahmed L and Poulikakos D 2009 *Langmuir* **26** 663–70
[32] Timofeeva E V, Gavrilov A N, McCloskey J M, Tolmachev Y V, Sprunt S, Lopatina L M and Selinger J V 2007 *Phys. Rev.* E **76** 061203
[33] Weitz D, Huang J, Lin M and Sung J 1984 *Phys. Rev. Lett.* **53** 1657
[34] Gerber R, Takayasu M and Friedlaender F 1983 *IEEE Trans. Magn.* **19** 2115–7
[35] Doyle P S and Underhill P T 2005 Brownian dynamics simulations of polymers and soft matter *Handbook of Materials Modeling* (Berlin: Springer) pp 2619–30
[36] Andreu J S, Calero C, Camacho J and Faraudo J 2012 *Phys. Rev.* E **85** 036709
[37] Andreu J S, Camacho J and Faraudo J 2011 *Soft Matter* **7** 2336–9
[38] Bombard A J, Joekes I and Knobel M 2003 *Mater. Sci. Forum* **416**
[39] Faraudo J and Camacho J 2010 *Colloid Polym. Sci.* **288** 207–15
[40] Chambon F and Winter H H 1987 *J. Rheol.* **31** 683–97
[41] Schneider F, Draheim J, Kamberger R and Wallrabe U 2009 *Sensors Actuators A* **151** 95–9
[42] Simoes B S F 2016 *Development of a Microfluidic Device for Blood Vessel Realization and Characterization* Bioengineering and Nanosystems
[43] Zhang J, Yan Y, Miao P and Cai J 2017 *Beilstein Journal of nanotechnology* **8**
[44] Mietta J, Negri R M and Tamborenea P I 2014 *J. Phys. Chem.* C **118** 20594–604